FACILE SYNTHESIS AND OPTIMIZATION OF GRAPHENE OXIDE REDUCTION BY ANNEALING IN HYDRAZINE VAPOUR IN AMBIENT AIR FOR POTENTIAL APPLICATION IN PEROVSKITE SOLAR CELLS

[1]Ochigbo Stephen Shaibu, * [2]Obar Alfred Obukohwo, [3]Suleiman M.A.T., [4]Kovo A.S.

[1]Department of Chemistry, Federal University of Technology, P.M.B. 65 Minna, Niger State, Nigeria
[2]Department of Chemistry, Federal University of Technology, P.M.B. 65 Minna, Niger State, Nigeria
[3]Department of Chemistry, Federal University of Technology, P.M.B. 65 Minna, Niger State, Nigeria
[4]Department of Chemical Engineering, Federal University of Technology, P.M.B. 65 Minna, Niger State, Nigeria

*Corresponding Author Email Address: fredology12@gmail.com

Phone: +2348035888263

ABSTRACT
Graphene oxide (GO) was synthesized from graphite via a modified Hummer's method, followed by thermal and chemical reductions to produce reduced graphene oxide (RGO) samples at various temperatures. A suite of characterization techniques including Fourier Transform Infrared Spectroscopy (FTIR), Scanning Electron Microscopy (SEM), Energy-Dispersive X-ray Spectroscopy (EDS), UV-Visible Spectroscopy, thermogravimetric analysis (TGA), X-ray diffraction (XRD), and Hall effect measurements were employed to assess the structural, morphological, optical, and electrical properties of the samples. FTIR analysis confirmed the successful functionalization of graphite to GO and subsequent reduction to reduced graphene oxide, with peak intensities decreasing as the reduction temperature increased. UV-visible spectroscopy of GO showed a maximum absorption at 235 nm which confirmed the synthesis of GO while the reduction revealed a notable red shift in absorption peaks with increasing annealing temperature, and that signified a reduction in bandgap. XRD analyses demonstrated the removal of oxygen functional groups. The X-ray diffraction (XRD) analysis of GO showed diffraction at $2\theta = 10.74°$ which revealed a fully oxidized graphene oxide with oxygen-containing functional groups, and hence an increase in interlayer spacing (d_{002}) from 3.341 Å (graphite) to 8.228 Å (GO). Upon reduction, there is a gradual decrease in d_{002} from 8.228 Å (GO) to 3.387 Å (HRGO300), suggesting the gradual removal of intercalated oxygen molecules, and hence the gradual restoration of sp^2 hybridisation in graphene. The EDS analysis revealed an increase in the carbon-to-oxygen (C/O) ratio from 1.78 in GO to 2.75 in HRGO300 as the annealing temperature for the reduction process increased which further confirmed the removal of oxygen functional groups. The Hall effect data showed hole mobility of 4.634×10^1 (GO), 4.831×10^1 (HRGO200), and 5.462×10^0 (HRGO300) with conductivities of 8.985×10^{-5} (GO), 1.087×10^0 (HRGO200) and 1.791×10^1 $1/\Omega$ cm, suggesting an increase in conductivity as the annealing temperature increased as revealed in the EDS. Out of the three samples identified as hole transport materials, the sample HRGO300 with the highest C/O ratio of 2.75 has the highest conductivity, and hence most suitable for application as hole transport material in perovskite solar cell.

Keywords: solar cell, graphene oxide, reduced graphene oxide, hole transport material.

INTRODUCTION
Graphene oxide (GO) has emerged as a promising material for various applications due to its unique properties, including its high surface area, excellent mechanical strength, and tunable electronic properties. Among the diverse methods employed for GO reduction, thermal reduction in hydrazine vapour has gained attention for its effectiveness in producing reduced graphene oxide (rGO) with enhanced conductivity and structural integrity. This literature review explores the synthesis and optimization of graphene oxide reduction by thermal reduction in hydrazine vapour, focusing on its potential application in solar cells.

Various methods have been developed for the synthesis of graphene oxide (GO). Brodie's method, dating back to 1859, involved the treatment of graphite with fuming nitric acid and potassium chlorate, laying the foundation for subsequent methods. Staudenmaier's method replaced nitric acid with a mixture of sulphuric acid and nitric acid, enhancing efficiency. The Hummers method (HM), developed in 1958, revolutionized GO synthesis by using a mixture of sulphuric acid, potassium permanganate, and other reagents. Tour's method introduced modifications to HM, increasing the yield of GO. Modified & improved Hummers methods (MHM) have since been developed to address limitations and improve efficiency, often by removing sodium nitrate and incorporating other catalysts. Recent advancements include multiple oxidations to tailor GO for specific applications and achieve higher yields.

Graphene oxide (GO) reduction is a crucial step in harnessing the full potential of graphene-based materials for various applications. In recent years, a wide array of reduction methods have been explored, including thermal, microwave, photo, chemical, electrochemical, and solvothermal approaches (Pei, 2012; Dreye, *et al., 2012*; Chua, *et al*., 2014, Obeta, 2013). Among these methods, thermal reduction in hydrazine vapour has emerged as a promising technique due to its simplicity, scalability, and effectiveness in producing rGO with enhanced properties.

Chemical reduction routes remain the most commonly applied methods for GO reduction, utilizing a diverse range of chemical compounds as reducing agents. Strong reducing agents such as hydrazine and its derivatives, metal hydrides, and hydroiodic acid are frequently employed, along with weaker reducing agents like ascorbic acid, hydroquinone, and alkaline solutions (Pei, 2012).

Facile Synthesis and Optimization of Graphene Oxide Reduction by Annealing in Hydrazine Vapour in ambient air for Potential Application in Perovskite Solar Cells

194

These chemical reduction methods offer versatility in controlling the degree of reduction and tailoring the properties of RGO for specific applications.

Reduced graphene oxide (rGO) exhibits significantly improved properties compared to GO, including higher conductivity, mechanical strength, and thermal stability. While GO behaves as an insulator due to defects and oxygen groups that isolate the sp^2 areas, rGO demonstrates substantially higher conductivity, making it ideal for various electronic and energy-related applications (Zhao *et al.,* 2012).

The optical properties of GO and rGO undergo significant alterations during the reduction process. GO exhibits characteristic absorption peaks in the ultraviolet range, attributed to $\pi \rightarrow \pi^*$ and $n \rightarrow \pi^*$ transitions in aromatic C=C and C=O bonds, respectively (Chen, 2013). Upon reduction to rGO, these transitions are modified, leading to changes in absorption intensity and spectrum broadening. The restoration of the sp^2 network in RGO results in increased absorption in the visible range, further enhancing its optical properties.

Thermal reduction in hydrazine vapour offers a straightforward and efficient method for producing RGO with desirable properties. This process involves exposing GO to hydrazine vapor at elevated temperatures, leading to the reduction of oxygen-containing functional groups and the restoration of the sp^2 network (Qiu, *et al.,* 2023). The reaction between hydrazine and GO results in the generation of nitrogen gas and water vapor, accompanied by a distinct color change in the solution, indicating the reduction process (Zhang, *et al.,* 2022).

Optimizing the synthesis of rGO through thermal reduction in hydrazine vapor involves fine-tuning various parameters such as temperature, reaction time, and precursor concentration. Higher temperatures and longer reaction times generally lead to increased reduction efficiency and conductivity of the resulting rGO (Sengupta, *et al.,* 2018). However, it is essential to balance these parameters to avoid structural damage and defects that may compromise the material's performance.

Characterizing the properties of RGO synthesized via thermal reduction in hydrazine vapour requires a combination of analytical techniques. Common characterization methods include X-ray photoelectron spectroscopy (XPS), Raman spectroscopy, atomic force microscopy (AFM), and X-ray diffraction (XRD) (Altaee, *et al.,* 2020). These techniques provide valuable insights into the chemical composition, structural integrity, and morphology of RGO, aiding in the optimization of synthesis parameters for specific applications.

The unique properties of RGO synthesized via thermal reduction in hydrazine vapour make it highly suitable for various applications, including solar cells. The enhanced conductivity, mechanical strength, and thermal stability of RGO make it an attractive candidate as a hole transport material in perovskite solar cells (Nowsherwan *et al.,* 2022).

Several methods have been used to prepare reduce graphene oxide, including heating to a very high temperature in vacuum or inert atmosphere, which is expensive and cumbersome. This investigation provides a facile route to moderate temperature reduction of graphene oxide in ambient condition, yet obtain fantastic results similar to heating at a high temperature in inert atmosphere or vacuum.

In conclusion, thermal reduction in hydrazine vapour offers a promising approach for the synthesis and optimization of reduced graphene oxide (rGO) with enhanced properties for potential application in solar cells. By fine-tuning the synthesis parameters and optimization strategies, researchers can tailor the properties of rGO films to meet the specific requirements of solar cell devices. Continued advancements in characterization techniques and optimization strategies will further accelerate the development of RGO-based solar cell technologies.

EXPERIMENTS

Preparation of graphene oxide and reduced graphene oxide
The preparation of graphene oxide and then reduced graphene oxide was carried out in three stages. The first step involved the oxidation of graphite powder, followed by the exfoliation of graphite oxide to form graphene oxide. The graphene oxide was then reduced by thermal reduction on the one hand, and, on the other hand, by chemical and thermal methods simultaneously. The oxidation of graphite powder produced graphite oxide; the exfoliation of graphite oxide produced graphene oxide; and the reduction of graphene oxide produced reduced graphene oxide.

Preparation of graphene oxide
Graphene oxide (GO) is produced from graphite powder using a modified Hummers' technique (Shahriary, *et al.,* 2014). A round bottom flask is kept in an ice bath and filled with 120.0mL H_2SO_4 (95%). Graphite powder (5.0 g) and $NaNO_3$ (2.5 g) are added to the flask under vigorous stirring. Following this step, 15.0 g $KMnO4$ is mixed under continued stirring at a temperature of less than 10 °C. After mixing $KMnO4$, the ice bath is taken off and the solution is stirred at 30 °C for over 24 hours. The mixture progressively grew thick (paste) and turned light brown. Following this, 150.0mL of deionized water was gradually added to this mixture under constant stirring. The diluted suspension was stirred for 2h at 98 °C. Subsequently, the temperature was decreased to 60°C, and 50.0 mL H_2O_2 (30%) was further added to the mixture to remove any leftover MnO_4^-, and then the colour of the suspension changed to bright yellow. Thereafter, 150 ml 1 M HCl (36%) was added to remove the sulphate and phosphate ions followed by centrifugation at 5000 rpm. The process was followed by washing with water ten times, and was each time centrifuged at 5000 rpm for 15 minutes until a solution with neutral pH was obtained, and was then sonicated for 4 hours. Thereafter, it was dried in an oven at 60 °C. A solution of 1 mg/ml was then prepared from the dried graphene oxide by dissolving 5 mg in 1 ml of solution and was then diluted five times to obtain 1mg/ml, and was labelled graphene oxide (GO)

Pretreatment of soda lime glass substrate
Soda-lime glass slides were cut into 1 x 1cm² and then watched with ethanol, rinsed with pure water, and immersed into a solution containing H_2SO_4 (98%) and H_2O_2 (30%) in a ratio of 3:1, a solution generally referred to as Piranha Solution. This process was carried out to rid the substrate of surface impurities. It was then allowed to dry in an oven at 30 °C for 30 minutes and then stored dried.

Facile Synthesis and Optimization of Graphene Oxide Reduction by Annealing in Hydrazine Vapour in ambient air for Potential Application in Perovskite Solar Cells

195

Preparation of thin films of graphene oxide and reduction of graphene oxide

GO thin films were prepared by spin coating at 2000 rpm for 30 s, and the graphene oxide thin films were reduced by thermal reduction in hydrazine hydrate vapour at 100, 200 and 300 °C. The reduction process was allowed to proceed for 30 minutes after reaching the respective temperatures. The heating is stopped and allowed to cool gradually on the hot plate before removing it. These samples were labelled HRGO100, HRGO200 and HRGO300 where HRGO means hydrazine vapour of reduction of graphene oxide at 100, 200, and 300 °C respectively, with a heating rate of 10 °C/min. The films were placed in a petri dish and covered with another petri dish and the temperature of the hotplate was set to the designated reduction temperature with 1 ml of hydrazine in the petri dish containing the thin films on soda lime glass.

Characterization

Characterization techniques Fourier transform infrared (FTIR) spectra of the samples were recorded on a ATR-FTIR (ATR-FTIR Cary 630, Japan). Ultraviolet-Visible (UV-Vis) spectra of the samples were collected on a UV-Vis spectrophotometer (Cary *60* UV-Vis Spectrophotometer, *Japan*). The X-ray diffraction analysis (XRD) of powders was carried out on an XRD diffractometer (Rigaku Mini Flex 600, Japan) with monochromatic CuKα, radiation (λ = 1.5406 A°). Data were collected from 10° to 60° at a scan rate of 0.1° min^{-1}. The mobility and conductivities of the samples were observed under (Hall Effect Analyzer, Lake Shore Cryotronics, Inc.).

RESULTS AND DISCUSSION

Functional group analysis of graphite and its derivatives

To confirm the functionalization of graphite to graphene oxide and the subsequent reduction of GO to reduced graphene, Figure 1 shows the FTIR spectra of the samples. The FTIR spectra revealed the presence of new peaks different from the precursor (graphite). The GO and HRGO 100°C samples showed peaks for the carboxyl C=O (1730 cm^{-1}), aromatic C=C (1638 cm^{-1}), epoxy C–O (1237 cm^{-1}), alkoxy C–O (1043 cm^{-1}), and hydroxy –OH (3402 cm^{-1}) groups. The presence of –OH broad peak suggests the hydrophilicity of graphene oxide, as a result of which GO can be dispersed in several solvents like water and ethanol (Stobinski, *et al.,* 2014).

The presence of oxygen-containing functional groups, such as C=O and C–O, further confirmed that the graphite was indeed oxidized into GO by the intercalation of oxygenated functional groups into the structure of graphite. This observation is consistent with the literature (Zhou, *et al.,* 2011; Zhang *et al.,* 2011; Shen *et al.,* 2011). It is evident that the characteristic peak for carboxyl C=O at 1735 cm^{-1} showed a much lower intensity for HRGO (Stobinski, *et al.,* 2014). These peaks are obviously reduced in RGO100, HRGO200 and HRGO300°C which suggests the removal of oxygen-containing functional groups.
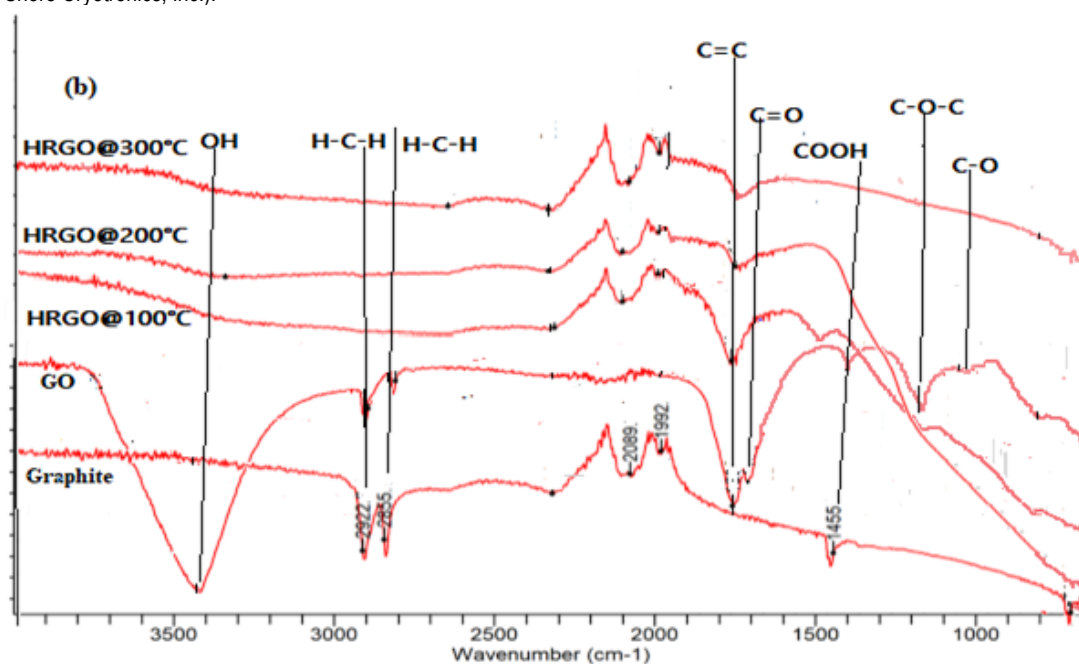

Figure 1: FTIR of graphite, GO, HRGO 100, HRGO 200, and HRGO 300

Ultraviolet (UV) visible spectrophotometer analysis of graphene oxide and reduced graphene oxides

Figure 2 shows UV-Vis absorbance of (a) GO and (b) HRGO samples. The GO shows maximum absorption at around 235 nm which is due to π to π* transition and corresponds to the aromatic C = C bonds, and a shoulder at around 300 nm corresponds to n to π* transition of GO. As the annealing temperature increases,

HRGO 100, 200 and 300 show a red shift towards a higher wavelength as the annealing temperature increases which suggest a shift towards a higher wavelength which implies a shift from higher energy of transition to a lower energy of n to π* due to a reduction in bandgap. This result is consistent with literature (Eluyemi *et al.,* 2016)
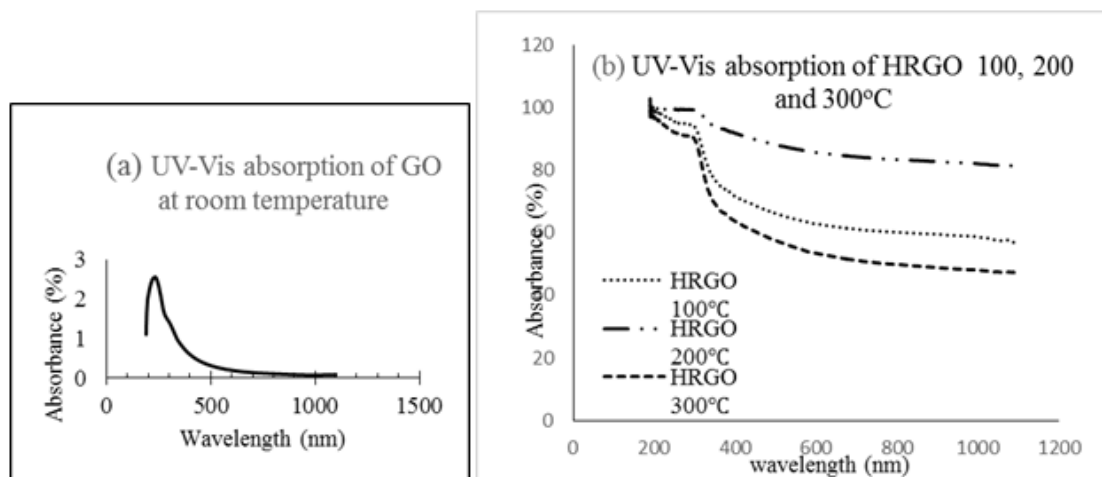
Facile Synthesis and Optimization of Graphene Oxide Reduction by Annealing in Hydrazine Vapour in ambient air for Potential Application in Perovskite Solar Cells

196

Figure 2: UV absorbance of (a) GO and (b) HRGO samplesA

X-ray diffraction (XRD) analysis of graphite and its derivatives
The phase identification of the sample thin films was analysed using X-ray diffraction (XRD; Rigaku Mini Flex) with a Cu Ka radiation (I = 1.540 Å) source operated at 40 kV and 30 mA in the range of 10–70°. Table 1 shows the data obtained from the XRD diffractogram of graphite, GO and HRGO, while Figure 3 shows the XRD diffractogram of graphite, GO, and HRGO at 100, 200, and 300 °C. The XRD diffractions at 2θ and the corresponding interlayer distances. Graphite shows a diffraction angle of 26.66° at an interlayer distance of 3.341 Å and graphene oxide shows a diffraction angle of 10.74° at an interlayer distance of 8.228 Å. The samples HRGO100, HRGO200, and HRGO300°C have the following major diffractions at 2θ as 23.06, 23.28, and 26.29°, respectively, and corresponding interlayer spacing of 3.854, 3.838, 3.838, 3.818, and 3.787 Å respectively. The diffraction angles decreased from graphite (26.66°) to graphene oxide (10.74°) and then increased from HRGO100°C (23.15°) to HRGO300°C (26.29°).

The behaviour observed in the XRD diffractions and the corresponding interlayer distances from graphite to graphene oxide and then to hydrazine vapour reduced graphene oxide (HRGO) revealed a highly reduced graphene oxide (HRGO) samples.
Graphite exhibits a diffraction peak at 26.66° with an interlayer distance of 3.341 Å, indicative of its well-ordered stacking of graphene layers. Graphene oxide displays a diffraction peak at 10.74° with a significantly larger interlayer distance of 8.228 Å. This increase is due to the introduction of oxygen-containing functional groups onto the graphene surface during the oxidation process, leading to interlayer-spacing increase and structural disruption.
Upon reduction, the oxygen-containing functional groups in graphene oxide are partially removed, resulting in the partial restoration of sp^2 carbon structure and a decrease in interlayer distance. The interlayer distances observed for HRGO samples (3.787 Å) are lower compared to graphene oxide, indicating a decrease in interlayer spacing as the reduction progressed. The decrease in interlayer distance from HRGO100°C to HRGO300°C suggests a further reduction in interlayer spacing as the annealing temperature increases. This indicates a more extensive removal of oxygen functional groups and enhanced graphitization of the carbon structure at higher temperatures.

Table 1: XRD of graphite, GO and HRGOs

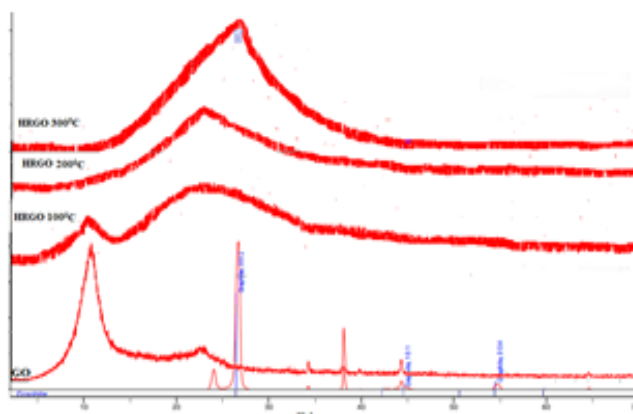| Sample	2θ (°)	Interlayer distance, d$_{002}$, (A)	Interlayer distance, d$_{002}$, (nm)
Graphite	26.66	3.341	33.41
GO	10.74	8.228	82.28
HRGO100°C	23.15	3.838	38.38
HRGO200°C	23.47	3.787	37.87
HRGO300°C	26.29	3.387	33.87

Figure 3: XRD diffractogram of graphite, GO and HRGO

Energy-dispersive X-ray spectroscopy analysis of graphite and its derivative Energy-dispersive X-ray spectroscopy (EDS) was used to analyse the oxygen content in the graphene oxide synthesized from graphite, and also to analyse the reduced graphene oxides for carbon-oxygen ratio in HRGO at 100, 200, and 300°C. From Table 2, the carbon-to-oxygen ratios for graphite, GO, HRGO100, HRGO200, and HRGO300°C are 26.91, 1.78, 1.94, 2.43, and 2.76.
The results obtained from Energy Dispersion Spectroscopy (EDS) analysis provide a valuable insight into the elemental composition

Facile Synthesis and Optimization of Graphene Oxide Reduction by Annealing in Hydrazine Vapour in ambient air for Potential Application in Perovskite Solar Cells

197

of the samples, particularly the carbon-to-oxygen (C/O) ratio. Graphite is primarily composed of carbon, with very little oxygen present. This high C/O ratio (26.91) is expected since graphite is a pure form of carbon with minimal impurities. The significantly low value in the carbon-oxygen ratio of the other samples compared to graphite indicates a substantial increase in oxygen content due to the oxidation process. Graphene oxide is produced by the oxidation of graphite, resulting in the introduction of oxygen-containing functional groups onto the graphene sheets.

For the carbon-oxygen ratio in HRGO at 100 (1.94), 200 (2.43), and 300 °C (2.76) samples, the trend observed suggests that increasing the annealing temperature in hydrazine hydrate vapour leads to a reduction of oxygen functional groups in the samples, and hence a gradual increase in the carbon-to-oxygen ratio. The trend observed in C/O agrees with the consequent of reduction of GO in literature (Zhang *et al.,* 2022).

Table 2: EDS of GO and HRGOs

Samples	Element (weight %)		C/O
	C	O	
Graphite	95.54	3.55	26.91
GO	61.97	34.81	1.78
HRGO@100°C	63.89	32.95	1.94
HRGO@200°C	65.39	26.89	2.43
HRGO@300°C	67.14	24.33	2.76

Electrical Conductivity and Resistivity
The electrical conductivity increases with an increase in annealing temperature (Table 4.4). This implies that the reduction of GO to RGO or HRGO leads to an increase in the conductivity of RGO and HRGO (Nyangiwe, *et al.,* 2015).

Table 3 shows the resistivity of the thin films as obtained from the Hall measurement. RGO 100 has the highest resistivity. For both RGOs and HRGOs, the resistivity of the thin films decreased with an increase in annealing temperature. This observation supports the fact that an increase in annealing temperature leads to a reduction of GO, and consequently a decrease in oxygen molar concentration. This is a departure from the insulating property attributed to GO as a result of the intercalating oxygen atoms separating the layers of graphene. Therefore, the reduction process will lead to a decrease in the oxygen concentration, and thus lead to an increase in conductivity. As the conductivity increases, the resistance decreases as a consequence of the decrease in insulating properties.

Table 3: Hall effect data of GO and HRGOs

Samples	Buck concentration (cm^{-3})	Mobility (cm^2/Vs)	Resistivity $(\Omega\ cm)$	Electrical Conductivity $(1/\Omega\ cm)$
GO	$1.210\ x10^{13}$	$4.634\ x10^1$	$1.113\ x10^4$	$8.985\ x10^{-5}$
HRGO 100°C	$-2.435\ x10^{16}$	$2.406\ x10^1$	$1.066\ x10^1$	$9.381\ x10^{-2}$
HRGO 200°C	$1.404\ x10^{17}$	$4.831\ x10^1$	$9.200\ x10^{-1}$	$1.087\ x10^0$
HRGO 300°C	$2.047\ x10^{19}$	$5.462\ x10^0$	$5.583\ x10^{-2}$	$1.791\ x10^1$

Charge carriers and mobility
Hall effect measurement is used to determine whether a material is an electron carrier or hole carrier, alongside other parameters such as mobility and conductivity. One other important factor, aside from the bandgap, that plays out in the efficiency of the solar cell is mobility and conductivity. In terms of hole mobility, it is expected to expedite the movement of the hole to the conduction band fast enough to guide against the duration and energy exhaustion of the excited hole. If the hole transport material does not move the hole fast enough before duration and energy exhaustion, the hole will return to the valence band of the perovskite and recombine with the electron to form an electron-hole pair.

From Table 3, the buck concentrations for GO, HRGO100, HRGO200, and HRGO300 are $1.210\ x10^{13}$, $-2.435\ x10^{16}$, $1.404\ x10^{17}$, and $2.047\ x10^{19}$ respectively, while the mobility are $4.634\ x10^1$, $2.406\ x10^1$, $4.831\ x10^1$, and $5.462\ x10^0$ cm²/Vs. The bulk concentration of the sample determines whether the sample is an electron transport material or not. When the bulk concentration is positive, the charge carrier of the sample is a hole transport material (p-type semiconductor), and when it is negative, the charge carrier of the sample is an electron (n-type semiconductor). From the buck concentration values, the hole transport materials are GO ($1.210\ x10^{13}$ cm⁻³), HRGO200 ($1.404\ x10^{17}$ cm⁻³), and HRGO300 ($2.047x10^{19}$ cm⁻³) while the electron transport material is HRGO100 ($-2.435\ x10^{16}$ cm⁻³). This research is primarily concerned with the hole transport materials, and no interest is vested in or associated with the samples that are electron transport materials.

Table 3 also shows the mobility and the corresponding electrical conductivity. The samples GO, HRGO100, HRGO200, and HRGO300°C have $4.634\ x10^1$, $2.406\ x10^1$, $4.831\ x10^1$, and $5.462\ x10^0$ cm²/Vs mobility respectively, while the conductivities are $8.985\ x10^{-5}$, $9.381\ x10^{-2}$, $1.087\ x10^0$, and $1.791\ x10^1$ 1/Ω cm respectively. Out of the three HTMs already identified, HRGO200°C has the highest mobility ($4.634\ x10^1$ cm²/Vs), the second is GO ($4.634\ x10^1$ cm²/Vs), and the least is RGO300°C ($5.462\ x10^0$ cm²/Vs), while the corresponding conductivities are $1.087\ x10^0$, $8.985\ x10^{-5}$, and $1.791x10^1$ 1/Ω cm, respectively. It becomes obvious that as the temperature increases, conductivity increases across the samples. However, the high value of mobility did not translate into high conductivity. The increase in conductivity is accounted for by the increase in the degree of reduction of the samples because an increase in the degree of reduction reduces the number of intercalated oxygen molecules, hence the increase in conductivity.

However, for the observed trend in mobility values, it is important to stress that efficient charge transport requires that the charges be able to transit from the valence band to the conduction band without being trapped or falling back to recombine. Therefore, charge carrier mobility is influenced by many factors, including molecular packing, disorder, the presence of impurities, temperature, electric field, charge-carrier density, size/molecular weight, and pressure. It would be too formidable a task to try to discuss all the experimental studies reported to date on the impact of these parameters on charge transport in organic semiconductors. However, the simplest and most common reason for this observation is polaron. In organic semiconductors, charge carriers are often localized in spatial regions called polarons due to

Facile Synthesis and Optimization of Graphene Oxide Reduction by Annealing in Hydrazine Vapour in ambient air for Potential Application in Perovskite Solar Cells

198

interactions with lattice vibrations (phonons). These interactions can reduce the effective mobility of charge carriers, leading to a discrepancy between mobility and conductivity (Coropceanu, *et al.,* 2015).

These values of mobility and conductivities meet the requirements of a hole transport material since the conductivity of the hole is > 10^{-4} S/cm and the hole mobility is > 10^{-5} cm^{2}V^{-1}s^{-1}. It is interesting to also state that these values supersede those of Spiro-OMeTAD and PEDOT:PSS, which were reported as 1.23 x 10^{-4} S/cm and 2.47 x 10^{-4} S/cm, respectively (Daniel *et al.,* 2019), and are currently leading in perovskite solar cells.

The mobility of Spiro-OMeTAD has been reported as 2 x 10^{-4} cm^2 V^{-1}s^{-1} (Poplavskyy and Nelson, 2003) and also reported as 2.2 x 10^{-4} cm^2 V^{-1}s^{-1} with a conductivity of 2.2 x 10^{-4} S/cm for Spiro-OMeTAD doped with LiTFSI in order to improve the conductivity.

In conclusion, graphene oxide was prepared by modified Hummer's method, while the reduced graphene oxide was made by thermal reduction of hydrazine hydrate vapour. The prepared graphene oxide and reduced graphene oxide were confirmed by FTIR, UV, and EDS. The suitability of the reduced graphene oxide was determined using Hall measurements and UV. The Hall measurements revealed the charge carriers, electrical conductivity, resistivity, and hole mobility. The GO, HRGO200, and HRGO300℃ are hole conductors, especially HRGO300℃, which has a mobility of 5.462 cm^2/ Vs and a conductivity of 17.91 1/Ω cm. The mobility value aligns with the standard (> 10^{-5} cm^2/ Vs) and is greater than the minimum standard by a wide margin. It also outwits Spiro-OMeTAD and many other hole transport materials in terms of hole mobility and conductivity. According to Leijtens (2013), the hole mobility of pristine Spiro-OMeTAD is 10^{-5} cm^2 V^{-1} s^{-1} while that of doped Spiro-OMeTAD is 10^{-3} cm^2 V^{-1} s^{-1}. Poplavskyy and Nelson (2003) reported values that are even lower for pristine Spiro-OMeTAD. Therefore, GO, HRGO200, and HRGO300℃ are all good hole transport materials that can be employed as hole transport materials in perovskite solar cells, but HRGO300℃ is far better because it has the highest conductivity. GO and HRGO200 could also be used but may require doping to improve the conductivity, especially GO.

REFERENCES

Altaee, H., Alshamsi, H. A. H., & Joda, B. A. (2020) Reduced graphene oxide supported palladium nanoparticles as an efficient catalyst for aerobic oxidation of benzyl alcohol. In AIP Conference Proceedings (Vol. 2290, No. 1, p. 030036). AIP Publishing LLC

Chaudhary, A. K., Verma, S., & Chauhan, R. K. (2023). Design of a low-cost, environment friendly perovskite solar cell with synergic effect of graphene oxide-based HTL and CH$_3$NH$_3$GeI$_3$ as ETL. *Engineering Research Express*, 5(3), 035039.

Chen, J.; Yao, B.; Li, C.; Shi, G. An improved Hummers method for eco-friendly synthesis of graphene oxide. Carbon 2013, 64, 225–229.

Chua, C. K, Pumera M (2014) Chemical reduction of graphene oxide: a synthetic chemistry viewpoint. Chem Soc Rev 43:291–312

Coropceanu, H.-S. Ko, J.-W. Lee, N.G. & Park, H. (2015) "15.76% Efficiency perovskite solar cells prepared under high relative humidity: importance of PbI$_2$ morphology in two-step deposition of CH$_3$NH$_3$PbI$_3$," *Journal of Materials Chemistry A*, 3, (16), 8808–8815.

Daniel, J. Borchert, H. Boht, W. Franzel, R. Csuk, R. Scheer, & P. Pistor (2015). "Structural investigation of co-evaporated methyl ammonium lead halide perovskite films during growth and thermal decom- position using different PbX2 (X = I, Cl) precursors, *Journal of Materials Chemistry A*, 3, (39), 19842–19849

Dreyer DR, Park S, Bielawski CW, Ruoff RS (2012) The chemistry of graphene oxide. Chem Soc Rev 39:228–240

Leijtens, G.; Sun S.; Cheetham, K. (2013) An extended Tolerance Factor Approach for Organic-Inorganic Perovskite. Chem. Sci., 6, 3430–3433.

Nowsherwan, G.A., Sabah, S. S., Khan, M., Akbar, I., Nadia, N., Ikram, S., Ishtiaq, S., Riaz, S., Naseem, S. (2023) Role of graphene-oxide and reduced-graphene-oxide on the performance of lead-free double perovskite solar cell. *Zeitschrift für Naturforschung A*, 77: 1083-1098.

Nyangiwe, S. Ye, W. Sun, Y. & Li, L. (2015). CuSCN-based inverted planar perovskite solar cell with an average PCE of 15.6%. *Nano Letters*, 15(6), 3723–3728.

Obata S, Tanaka H, Saiki E (2013) Electrical and spectroscopic investigations on the reduction mechanism of graphene oxide. Carbon 55:126–132

Pei S, Cheng H-M (2012) The reduction of graphene oxide. Carbon 50:3210–3228

Poplavskyy, G. & Nelson, J. K. (2003). Quantum dot solar cells. The next big thing in photovoltaics, *Journal of Physical Chemistry Letters*, 4, (6), 908–918.

Qiu, C., Jiang, L., Gao, Y., & Sheng, L. (2023, June). Effects of oxygen-containing functional groups on carbon materials in supercapacitors: A review. *Materials & Design*, 230, 111952. https://doi.org/10.1016/j.matdes.2023.111952

Sengupta, I., Chakraborty, S., Talukdar, M., Pal, S. K., & Chakraborty, S. (2018). Thermal reduction of graphene oxide: How temperature influences purity. *Journal of Materials Research*, *33*(23), 4113–4122. https://doi.org/10.1557/jmr.2018.338

Shahriary, L. & Athawale, A.A. (2014) Graphene Oxide Synthesized by Using Modified Hummers Approach. International Journal of Renewable Energy and Environmental Engineering, 2, 58-63.

Stobinski L, Lesiak B, Malolepszy A, Mazurkiewicz M, Mierzwa B, Zemek J, Jiricek P, Bieloshapka I (2014) Graphene oxide and reduced graphene oxide studied by the XRD, TEM and electron spectroscopy methods. J Electron Spectros Re Phenom 195:145–154

Stobinski, A. Kojima, K. Teshima, Y. Shirai, T. & Miyasaka, D. (2014). Novel pho- toelectrochemical cell with mesoscopic electrodes sensitized by lead-halide compounds (11), *Meeting Abstract,* MA2008-02 27, no. 1, 27.

Zhang, Q., Yang, Y., Fan, H., Feng, L., Wen, G., & Qin, L. C. (2022). Synthesis of graphene oxide using boric acid in hummers method. *Colloids and Surfaces A: Physicochemical and Engineering Aspects*, *652*, 129802. https://doi.org/10.1016/j.colsurfa.2022.129802

Zhao, B.; Liu, P.; Jiang, Y.; Pan, D.; Tao, H.; Song, J.; Fang, T.; Xu, W. Supercapacitor performances of thermally reduced graphene oxide. J. Power Sources 2012, 198, 423–427.

Facile Synthesis and Optimization of Graphene Oxide Reduction by Annealing in Hydrazine Vapour in ambient air for Potential Application in Perovskite Solar Cells

199